APL Materials

Signatures of temperature driven antiferromagnetic transition in the electronic structure of topological insulator $MnBi_2Te_4$

Cite as: APL Mater. **8**, 021105 (2020); https://doi.org/10.1063/1.5142846
Submitted: 19 December 2019 . Accepted: 21 January 2020 . Published Online: 06 February 2020

D. A. Estyunin, I. I. Klimovskikh, A. M. Shikin, E. F. Schwier, M. M. Otrokov, A. Kimura, S. Kumar, S. O. Filnov, Z. S. Aliev, M. B. Babanly, and E. V. Chulkov

Signatures of temperature driven antiferromagnetic transition in the electronic structure of topological insulator $MnBi_2Te_4$

Cite as: APL Mater. 8, 021105 (2020); doi: 10.1063/1.5142846
Submitted: 19 December 2019 • Accepted: 21 January 2020 •
Published Online: 6 February 2020

D. A. Estyunin,[1,a] I. I. Klimovskikh,[1] A. M. Shikin,[1] E. F. Schwier,[2] M. M. Otrokov,[3,4] A. Kimura,[5] S. Kumar,[2] S. O. Filnov,[1] Z. S. Aliev,[6,7] M. B. Babanly,[8,9] and E. V. Chulkov[1,10,11,12]

AFFILIATIONS

[1] Saint Petersburg State University, Saint Petersburg 198504, Russia
[2] Hiroshima Synchrotron Radiation Center, Hiroshima University, Hiroshima, Japan
[3] Centro de Fisica de Materiales (CFM-MPC), Centro Mixto CSIC-UPV/EHU, Donostia-San Sebastian, Basque Country, Spain
[4] IKERBASQUE, Basque Foundation for Science, Bilbao E-48011, Basque Country, Spain
[5] Department of Physical Sciences, Graduate School of Science, Hiroshima University, Hiroshima, Japan
[6] Azerbaijan State Oil and Industry University, Baku, Azerbaijan
[7] Institute of Physics, National Academy of Sciences of Azerbaijan, Baku, Azerbaijan
[8] Institute of Catalysis and Inorganic Chemistry, Azerbaijan National Academy of Science, Baku, Azerbaijan
[9] Baku State University, Baku, Azerbaijan
[10] Donostia International Physics Center (DIPC), Donostia-San Sebastian, Basque Country, Spain
[11] Departamento de Física de Materiales UPV/EHU, 20080 Donostia-San Sebastián, Basque Country, Spain
[12] Tomsk State University, 634050 Tomsk, Russia

[a] **Author to whom correspondence should be addressed:** estyunin@gmail.com

ABSTRACT

In this work, we employed angle resolved photoemission spectroscopy (ARPES) to analyze the temperature dependent changes in the electronic structure of the first antiferromagnetic topological insulator $MnBi_2Te_4$ upon crossing the Néel temperature $T_N \approx 25$ K. We observed an exchange splitting of the bulk conduction band, which has a power law dependence on temperature $(1 - T/T_0)^{2\beta}$ with an onset temperature T_0 well matching the measured bulk T_N. We found a matching temperature evolution of the topological surface states integrated spectral weight in the vicinity of the Dirac point. Furthermore, we observed an additional quasi-2D state with Rashba-type splitting, which is also affected by the emerged magnetism and exhibits an opening of a gap, reminiscent of the effect of an out-of-plane magnetic field, below T_N. All these findings point toward strong evidence of the interplay between emerged magnetism with bulk and topological surface states. The observed temperature-dependent effects in $MnBi_2Te_4$ may be used as an experimental fingerprint for the presence of magnetism and may guide the future analysis of ARPES spectra in magnetic topological insulators.

A combination of magnetic and topological orders in novel quantum materials has unlocked an intriguing research area in condensed matter physics. Breaking of time reversal symmetry (TRS) in 3D topological insulators (TI) has been recently proposed to be the way to realize the quantum anomalous Hall effect (QAHE).[1] When TRS is broken via exchange interactions, the topological surface states (TSS) are no longer protected, and a gap opens at the Dirac point (DP).[2,3] This leads to the creation of chiral 1D edge states with quantized Hall resistance. Magnetism can be induced into TIs in the following ways: doping with magnetic atoms,[4,5] via

a proximity effect,[6,7] magnetic extension of TI crystal structure,[8–10] or the creation of intrinsic magnetic TI.[11–13] To this date, the most common way[1,2,14–22] and the only one with experimentally observed QAHE[1,16] is doping of 3D TI $(Bi,Sb)_2(Te,Se)_3$ with magnetic 3d or 4f elements. However, the highest observed critical temperature required for QAHE has been limited to 1 K,[23] which could be caused by the arbitrary localization of magnetic atoms.[24] The temperature of the TI transition to the QAHE regime is expected to be related to the size of the bandgap at the DP and the TI's magnetic ordering temperature.[3,25] Therefore, the recently discovered intrinsic antiferromagnetic (AFM) TI $MnBi_2Te_4$ (MBT)[9,11,26–33] has a great potential to show a high-temperature QAHE.

Indeed, it was shown that MBT is characterized by a high Néel temperature (T_N) and a large bandgap at the DP in comparison with magnetically doped TIs. The material has a layered structure and consists of septuple layer (SL) blocks (Te–Bi–Te–Mn–Te–Bi–Te) stacked along the c axis and separated by van der Waals gaps. From magnetic measurements, it was shown that MBT exhibits an A-type AFM ordering with an easy axis perpendicular to the layers, i.e., parallel to c.[11,34] According to theoretical calculations and direct magnetic measurements, T_N of MBT is about 25 K.[11,35,36] Below T_N, theory predicts an opening of a giant bandgap of ~80 meV at the DP in case of A-type AFM ordering. Experimentally such order gaps for MBT have been reported in Refs. 11, 37, and 38. However, several recent experiments propose small gap (<20 meV),[39,40] which is explained in terms of a deviation of the surface magnetic ordering from the bulk. These deviations are suggested to be caused by reconstruction processes and sensitivity to surrounding environments. This inconsistency of results indicates the possibility of a complex space-varying magnetic structure in MBT. Therefore, a more detailed investigation of the system's evolution processes in respect to the emerged magnetic state is required.

With this intention, here we present a detailed study of the electronic structure in paramagnetic (PM) and AFM phases in MBT by means of μ-focused Laser-based angle resolved photoemission spectroscopy (ARPES).[41] We demonstrate that both the bulk conduction band (BCB) states and the topological surface state (TSS) spectral weight are affected by the emerged magnetism.

ARPES above and below the AFM transition temperature: We first analyze the MBT band structure well above and below T_N (Fig. 1). The spectra $N(E)$ in Figs. 1(a) and 1(b), accompanied with their second derivatives d^2N/dE^2 in Figs. 1(c) and 1(d), show dispersion maps $E(k_x)$ measured along the $\overline{\Gamma K}$ high symmetry direction of the surface Brillouin zone. In Fig. 1(a), one can identify a band marked by the green dashed line (A), which is clearly visible in the second derivative in (c). According to *ab initio* calculations,[11] this state corresponds to the bottom of the BCB and has a weak dispersion along the k_z direction. Figure 1(b) shows the band structure below T_N. The original single band (A) now visibly splits into two bands, marked with red and blue curves and labeled as (B) and (C).

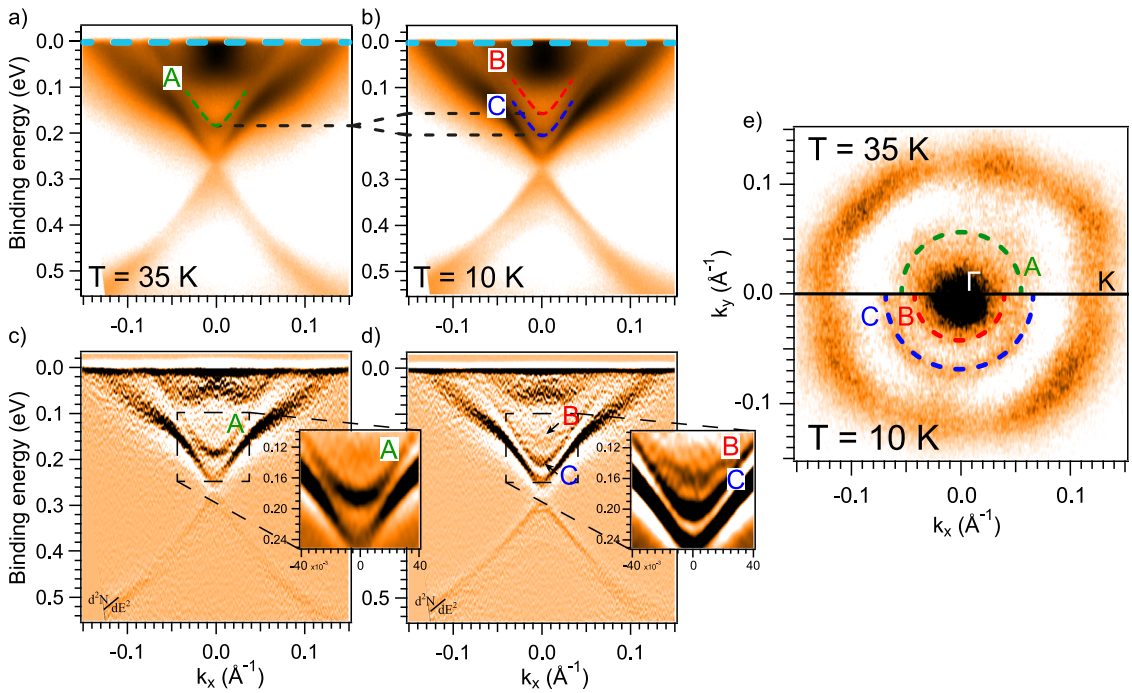

FIG. 1. (a) and (b) Band dispersions $E(k_x)$ of AFMTI MBT measured along the $\overline{\Gamma K}$ direction with photon energy of 6.3 eV at T = 35 K and T = 10 K, respectively. Green, red, and blue dashed curves with corresponding labels (A)–(C) in (a) and (b) show states of interest. The green curve marks the degenerated (A)-band above T_N, and blue and red curves mark the (B) and (C) bands after splitting occurs below T_N. Black horizontal lines correspond to the minimum of highlighted bands and schematically show splitting process. (c) and (d) demonstrate the second derivative d^2N/dE^2 of spectra (a) and (b), respectively. Insets in (c) and (d) focus on the region of the split states. Cyan lines near the Fermi level mark the position of constant energy cuts in (e). Here, the bottom part corresponds to the one half (in k-space) of the Dirac cone at T = 10 K, and the upper part to the second half at T = 35 K. The Fermi surface map was obtained by combining a number of band dispersions $E(k_x)$ at various emission angles corresponding to different k_y. It is presented as a second derivative for better visualization. Blue, red, and green half circles correspond to the same bands as in (a) and (b).

Despite its weak intensity, the lower binding energy band (B) can be observed in the second derivative plot [Fig. 1(d) and its inset] as well as in the energy distribution curves (EDC) in Fig. 2(c). The splitting is also clearly visible as a modification of the Fermi surface, as shown in Fig. 1(e) where states of interest are highlighted with the same colors and labels as in Figs. 1(a) and 1(b).

Temperature dependence of the band splitting: In order to track the evolution of MBT electronic structure across the AFM/PM transition, we measured a detailed set of dispersion curves $E(k_x)$ heating the sample from 10 K to 35 K and cooling back to 10 K. The measurements upon heating and cooling exhibit essentially the same behavior, proving the absence of aging effects on the measurements. To improve the statistics and precision of our analysis, we show the average results for each temperature point. First, we focus on the bottom state of the BCB (A) highlighted in Fig. 1 with green. Experimental EDC obtained at the $\bar{\Gamma}$-point at various temperatures (10–35 K; step 0.5 K) are presented in Fig. 2(a) as the second derivative (d^2N/dE^2) for better visualization [for $N(E)$ see the supplementary material, Fig. 1S]. One can clearly see that the band (A) splits into two (B) and (C) upon crossing $T \approx 25$ K. Starting from low temperatures, at which bands (B) and (C) are well separated, we use two Voigt profiles to describe the bands of interest and fit the EDCs. The resulting binding energies of (B) and (C) are plotted in Fig. 2(b) as red and blue dots. At 10 K, the states are well separated by ≈45 meV and move closer to their common center of mass with elevated temperatures. Above 23 K, the two-peak fit breaks down as the binding energies become comparable with each other. To track the evolution within the PM phase, we reduce the number of Voigt profiles to one and start fitting from the well defined electronic structure at 35 K, moving toward the PM/AFM transition temperature. The resulting binding energies are again plotted in Fig. 2(b) as green dots. This time, peak's binding energy is unchanged, and no temperature dependence is visible above T_N. In Fig. 2(c), we present a precise analysis of the fitting components including the Dirac cone, bulk valence, and described above bulk conduction bands. The profiles in Fig. 2(c) bottom and top parts are cut from the $E(k_x)$ dispersions in Figs. 1(a) and 1(b), correspondingly. Except for the main peaks of interest, related to the BCB states (A) at 35 K and (B) and (C) at 10 K, we used additional six peaks describing the other bands within the range of the EDCs: cyan and magenta for the Dirac cone states, gray for valence and upper part of BCB.

Having obtained the binding energy of the split bands as a function of temperature, we perform a fitting of the temperature dependence of the splitting in Fig. 2(b). Assuming the splitting is of exchange-type related to the magnetic long range order of the sample, the energy splitting should exhibit a linear dependence on the magnetic moment ($\Delta E \sim \mu$) and would be well described via a standard power law $\mu \sim (1 - T/T_0)^{2\beta}$. The results of the fitting are added to Fig. 2(b) as black dashed lines and well match

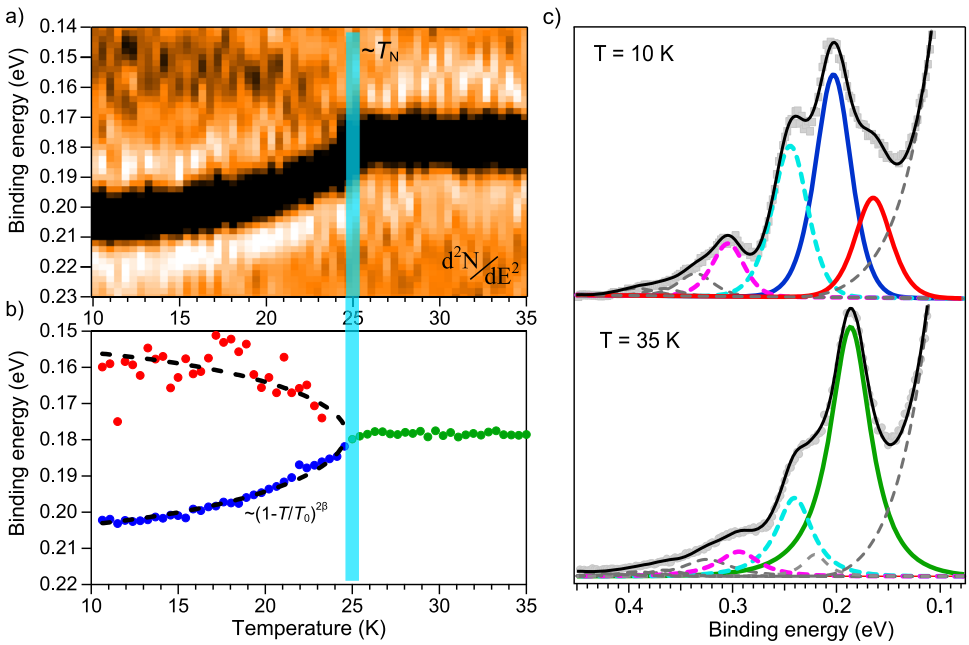

FIG. 2. (a) Set of experimental EDCs taken at the $\bar{\Gamma}$-point in the temperature range between 10 K and 35 K and step ΔT = 0.5 K, presented as $d^2N(E)/dE^2$. (b) Dots mark positions of the split BCB states as a function of temperature: green—(A), red—(B), and blue—(C). Black dashed lines show approximation below T_0 of the experimental data using a power-law-type behavior $\sim E_0 \cdot (1 - T/T_0)^{2\beta} + E_A$. Here, E_0 represents the saturated exchange splitting energy at T = 0 K, and E_A is an energy offset corresponding to the position of the degenerated (A)-state marked with green. The vertical cyan line in (a) and (b) points T_N. (c) Spectral decomposition of the EDCs at the $\bar{\Gamma}$ point at T = 10 K (top part) and T = 35 K (bottom part). Gray circles (bottom) and squares (top) represent experimental points, black solid lines are fitted functions, and gray lines represent additional spectral components (see the text). Magenta and cyan peaks correspond to components of the Dirac cone. The green peak (bottom panel) is for (A)-state above T_N and blue and red peaks (top panel) are for split states (B) and (C) below T_N.

the observed temperature dependence. Fitting parameters give values T_0 = 24.8 ± 0.3 K and $\beta \approx 0.25$. From an extrapolation of the fit function, we extract a saturated exchange splitting of 55 meV at 0 K (at 10 K to ~45 meV). The AFM transition temperature T_N as extracted from susceptibility measurements[11] and onset temperature T_0 estimated from our ARPES experiments match well within their respective errors. A power law behavior with similar parameters of T_0 and β was also found for the intensity of the reflection peak related to the AFM structure in neutron scattering in MBT compound.[34]

In the case of antiferromagnetically ordered MBT (A-type AFM, along *c*-axis), the splitting of the BCB state also can be found in density functional theory (DFT) calculations of the MBT band structure.[11,39] These calculations reveal two parabolic bands which are located above the upper part of the Dirac cone state. The bands are split for about 60–65 meV that slightly exceeds our estimation of the splitting saturation of 55 meV (at $T = 0$ K). In the PM phase (Ref. 39), no splitting is predicted for the BCB, and the mentioned bands are merged at their center of mass similar to what is observed in our experiment (e.g., Figs. 1 and 2). Based on comparison with DFT,[28] we assume that the BCB (A)-state has mostly the Te p-type character. It was shown that the magnetic moment can be induced on Te atoms by 3*d* magnetic elements, as it was demonstrated for V doped TI.[42] Furthermore, assuming a free-electron-like parabolic band dispersion, a splitting of ~50 meV would correspond to an internal field of about 400 T.[43] Local fields of such strength are typically refereed to magnetic materials.

Together, these results allow for an unambiguous interpretation of exchange-energy driven lifting of spin degeneracy for the band (A) below the bulk PM/AFM transition temperature. The most important here is that the splitting onset temperature matches with bulk T_N, which gives potential to probe magnetic properties of MBT compound simultaneously with electronic structure at the same position.

Exchange splitting in Rashba-like states: In the region close to the Fermi level, one can observe an additional conduction band state that is presented by two parabolas, shifted symmetrically along the wave vector. Such a behavior is reminiscent of the Rashba-like splitting in quasi-2D conduction band states. This Rashba-like band is better visible in the zoomed region of Figs. 1(c) and 1(d) presented in Figs. 3(a) and 3(b) as the second derivative d^2N/dE^2. To analyze this band behavior, we make an approximation of the state's intensity maxima, by a Rashba-type function with an exchange-interaction term $E_{\pm}(k) \sim \frac{\hbar k^2}{2m^*} \pm \sqrt{(\alpha_R k)^2 + \Delta^2}$.[44] Written in such form $E_{\pm}(k)$ has two parts where "−" corresponds to the dispersion below the parabolas crossing point [i.e., Kramers' point (KP)] and "+" is for the part above it. Here, α_R is the Rashba parameter, m^* is the effective mass, and 2Δ is the size of bandgap at the KP. Approximation of the ARPES dispersion with $E_-(k)$ is shown with green thick lines in Figs. 3(a) and 3(b). The part lying above the KP is close to the Fermi level and weakly resolved. Therefore, we reproduce it (shown with green thin lines) using $E_+(k)$ with parameters obtained for the $E_-(k)$. One can see that for $T = 35$ K, the model curves with $\Delta = 0$ eV match the experimental density distribution well. Therefore, we can assume an absence of a bandgap at the KP within the PM phase. However, at $T = 10$ K in the AFM phase, the density distribution of the band changes and a bandgap appears to be open with a size of about 30 meV. Additional evidence of the gap opening can be seen in the $N(E)$ profiles, cut at the $\bar{\Gamma}$-point, Fig. 3(c). Density distribution in vicinity of the Fermi level becomes flatter moving from 35 K to 10 K and its maximum shifts by roughly 15 meV (red and blue arrows, correspondingly). From the temperature evolution of the band, we found that the KP bandgap size is temperature dependent and has onset temperature similar with the one of the BCB (A), i.e., T_N [see Fig. 2S(a,b)].

Since the Rashba-like band is located in the region of the BCB, we can describe it as quasi-2D bulk state or surface resonance. A very similar Rashba-split state can be found in theoretical *ab initio* calculations[39] corresponding to the AFM phase. Surprisingly, calculations do not reveal any KP bandgap opening in the AFM phase. Thus, the Rashba-like state appearing in our experiment and the one predicted by calculations may be different in nature.

Temperature dependence of the Dirac cones spectral weight: Finally, we analyze the TSS's response to the magnetic ordering. While theory undoubtedly predicts an opening of a giant bandgap up to 90 meV for A-type AFM ordering, experimental results have a wide variation from narrow gapped (<20 meV) states[39] to rather pronounced DP bandgap.[11] Here we extend our findings in regard to the Dirac cone intensity variation with temperature presented in Ref. 11.

One can see that in the AFM phase [Fig. 1(b)], edges of the TSS are more pronounced than in the case within the PM phase [Fig. 1(a)]. This has significant effect on the precision of the bandgap

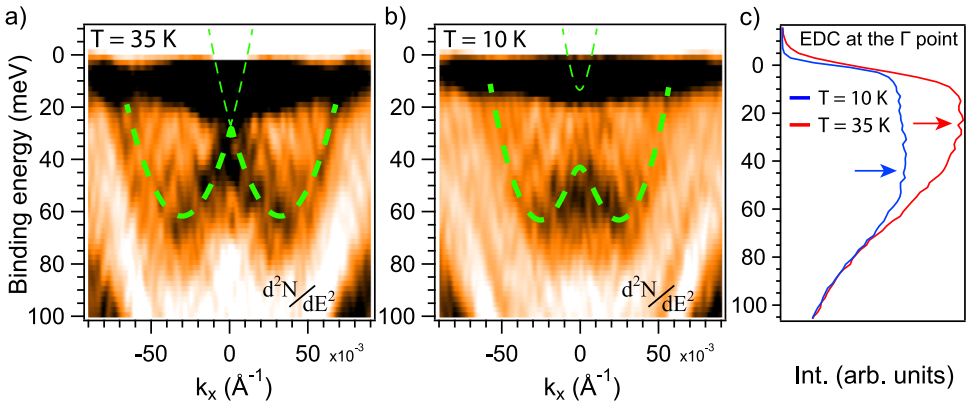

FIG. 3. (a) and (b) Zoomed region of Figs. 1(c) and 1(d) near the Fermi level, presented as the second derivative d^2N/dE^2. Green dashed lines show approximation of density maxima with energy distribution function of Rashba-type splitting $E_{\pm}(k)$. From the fitting Rashba parameter, a_R is 2.2–2.5 eV·Å and the KP bandgap 2Δ is 0 meV at 35 K (a) and ~30 meV at 10 K (b). (c) EDCs at the $\bar{\Gamma}$-point cut from $N(E)$ spectra at T = 35 K (red) and T = 10 K (blue). Arrows show corresponding density maxima [see Figs. 2S(c) and 2S(d) for spectral decomposition].

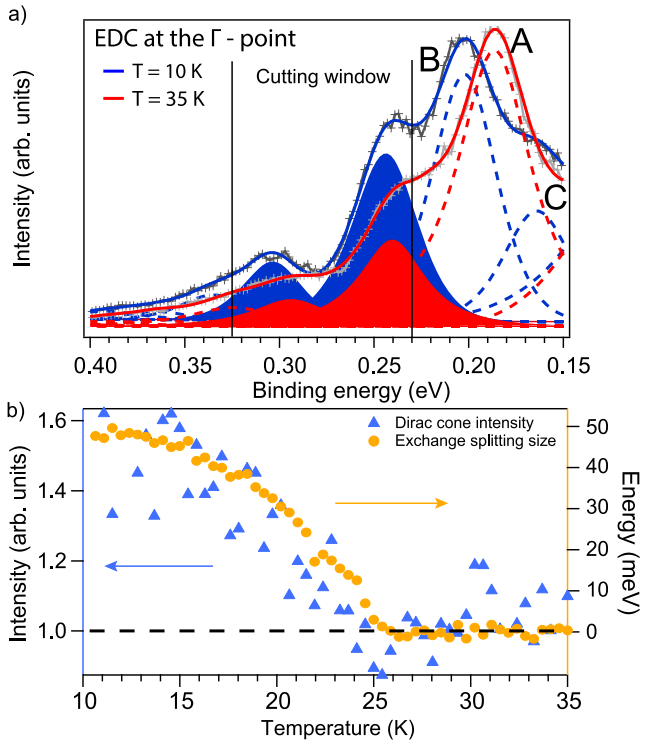

FIG. 4. (a) Direct comparison between spectra from Fig. 2(c) measured at 35 K (shown in red color and light gray) and 10 K (shown in blue color and dark gray). Labels (A)–(C) mark states in correspondence with Fig. 1. Solid peaks show spectral components of low and upper Dirac cone parts. (b) Integrated intensity of the TSS in the vicinity of the DP within temperature region between 10 K and 35 K is shown with blue triangles. The TSS average intensity at the plateau region (above T = 25 K) is set to 1. For the comparison temperature evolution of BCB, (A)-state exchange splitting size is added as yellow circles. Here, the splitting size is presented as doubled value of bottom brunch [blue in Fig. 2(b)].

estimation. The spectrum at T = 10 K [Fig. 4(a) blue curves] in the vicinity of the DP can be decomposed with two clearly separated peaks (solid blue), which reveal a gap size of 60 meV. However, at elevated temperatures [T = 35 K; Fig. 4(a) red curves], the peak decomposition is rather ambiguous and can be influenced by either of the following: a closing of the gap or a broadening of the peaks. The current fit returns a reduction of the DP gap by roughly 15 meV. The fitting was done at an almost constant peak width, which is the only one possible case [see Methods (supplementary material) for the fitting process]. Nevertheless, one can clearly see that peaks' intensity drops significantly between T = 10 K and T = 35 K.

To track the intensity evolution between these two points, we make temperature dependent analysis of the total spectral weight of the TSS near the DP. It is done by integrating intensity of spectra $E(k)$ at each temperature point within a window of $\Delta E \approx 100$ meV [Fig. 4(a)] and $\Delta k = 0.01$ Å^{-1}. Such a cutting window mostly includes the Dirac cone spectral components (see the Spectra analysis in the Methods section in the supplementary material).

Resulting dependence of the TSS intensity on the temperature is shown with blue triangles in Fig. 4(b). The TSS intensity in the AFM phase at T = 10 K is ~60% larger than in the PM phase. This points to a significant change in the TSS upon the AFM/PM transition.

The value of the BCB (A)-state exchange splitting is added to Fig. 4(b). One can see that both dependencies well match each other regarding onset temperature T_0 and overall behavior. Therefore, the TSS intensity also seems to be dominated by the power law dependence on temperature as the exchange splitting of BCB state (A). At the same time, the integrated intensity of states in BCB (Fig. 3S) stays constant with temperature. From these facts, we can establish that the Dirac cone spectral weight is influenced by the presence of the AFM phase. This finding could be a very important result since it may be the direct evidence for an interaction between the Dirac cone states and magnetic phase in the MBT system.

In conclusion, our results demonstrate the explicit variation of the electronic structure of AFMTI MBT across the AFM/PM transition temperature. By means of high energy resolution ARPES, we observe the evolution of an exchange splitting within the electronic structure of the bulk conduction band with its onset temperature well matches to the bulk AFM ordering temperature T_N = 25 K. This finding enables simultaneous estimation of the electronic and magnetic properties in MBT compound, which can shed light on a problem of electronic states response to the antiferromagnetic ordering. Additionally, we found a Rashba-like state within the conduction band that demonstrates an opening of a bandgap at the Rashba parabolas crossing point below T_N. We further observe an increase of the Dirac cone spectral weight with power law behavior on temperature below T_N, which claims of interplay between magnetism and the Dirac cone state. Therefore, our results reveal the response of different states of BCB and TSS to the antiferromagnetic ordering. Most importantly, this response is not the same for the topological surface and bulk conduction band states. Further investigations are required to study the direct interplay between the magnetism and topology in the novel intrinsic magnetic topological insulators.

Note added in proof. During preparation of this project, we became aware that the other group[40,45] also independently observed the effect of the bulk conduction band splitting in $MnBi_2Te_4$ below T = 25 K.

See the supplementary material for more details on the experimental methods, spectra analysis, and crystal growth.

The authors acknowledge support from the Saint Petersburg State University (Grant No. 51126047), the Russian Science Foundation (Grant No. 18-12-00062), and the Russian Foundation for Fundamental Investigations (No. 20-32-70179). The ARPES experiments were performed at HiSOR under Proposal Nos. 18BG026 and 18BU006. A. Kimura was financially supported by KAKENHI (Grant Nos. 17H06138, 17H06152, and 18H03683). Z. S. Aliev and M. B. Babanly acknowledge support from the Science Development Foundation under the President of the Republic of Azerbaijan (Grant No. EIF/MQM/Elm-Tehsil-1-2016-1(26)-71/01/4-M-33). The support by Tomsk State University competitiveness improvement program (No. 8.1.01.2018) is gratefully acknowledged.

REFERENCES

[1] C.-Z. Chang, J. Zhang, X. Feng, J. Shen, Z. Zhang, M. Guo, K. Li, Y. Ou, P. Wei, L.-L. Wang, Z.-Q. Ji, Y. Feng, S. Ji, X. Chen, J. Jia, X. Dai, Z. Fang, S.-C. Zhang, K. He, Y. Wang, L. Lu, X.-C. Ma, and Q.-K. Xue, Science **340**, 167 (2013).

[2] Y. L. Chen, J.-H. Chu, J. G. Analytis, Z. K. Liu, K. Igarashi, H.-H. Kuo, X. L. Qi, S. K. Mo, R. G. Moore, D. H. Lu, M. Hashimoto, T. Sasagawa, S. C. Zhang, I. R. Fisher, Z. Hussain, and Z. X. Shen, Science **329**, 659 (2010).

[3] C.-Z. Chang and M. Li, J. Phys.: Condens. Matter **28**, 123002 (2016).

[4] R. Yu, W. Zhang, H.-J. Zhang, S.-C. Zhang, X. Dai, and Z. Fang, Science **329**, 61 (2010).

[5] J. G. Checkelsky, J. Ye, Y. Onose, Y. Iwasa, and Y. Tokura, Nat. Phys. **8**, 729 (2012).

[6] X.-L. Qi, T. L. Hughes, and S.-C. Zhang, Phys. Rev. B **78**, 195424 (2008).

[7] I. Vobornik, U. Manju, J. Fujii, F. Borgatti, P. Torelli, D. Krizmancic, Y. S. Hor, R. J. Cava, and G. Panaccione, Nano Lett. **11**, 4079 (2011).

[8] T. Hirahara, S. V. Eremeev, T. Shirasawa, Y. Okuyama, T. Kubo, R. Nakanishi, R. Akiyama, A. Takayama, T. Hajiri, S.-i. Ideta, M. Matsunami, K. Sumida, K. Miyamoto, Y. Takagi, K. Tanaka, T. Okuda, T. Yokoyama, S.-i. Kimura, S. Hasegawa, and E. V. Chulkov, Nano Lett. **17**, 3493 (2017).

[9] M. M. Otrokov, T. V. Menshchikova, M. G. Vergniory, I. P. Rusinov, A. Yu Vyazovskaya, Y. M. Koroteev, G. Bihlmayer, A. Ernst, P. M. Echenique, A. Arnau, and E. V. Chulkov, 2D Mater. **4**, 025082 (2017).

[10] M. M. Otrokov, T. V. Menshchikova, I. P. Rusinov, M. G. Vergniory, V. M. Kuznetsov, and E. V. Chulkov, JETP Lett. **105**, 297 (2017).

[11] M. M. Otrokov, I. I. Klimovskikh, H. Bentmann, D. Estyunin, A. Zeugner, Z. S. Aliev, S. Gaß, A. U. B. Wolter, A. V. Koroleva, A. M. Shikin, M. Blanco-Rey, M. Hoffmann, I. P. Rusinov, A. Y. Vyazovskaya, S. V. Eremeev, Y. M. Koroteev, V. M. Kuznetsov, F. Freyse, J. Sánchez-Barriga, I. R. Amiraslanov, M. B. Babanly, N. T. Mamedov, N. A. Abdullayev, V. N. Zverev, A. Alfonsov, V. Kataev, B. Büchner, E. F. Schwier, S. Kumar, A. Kimura, L. Petaccia, G. Di Santo, R. C. Vidal, S. Schatz, K. Kißner, M. Ünzelmann, C. H. Min, S. Moser, T. R. F. Peixoto, F. Reinert, A. Ernst, P. M. Echenique, A. Isaeva, and E. V. Chulkov, Nature **576**, 416 (2019).

[12] J. Wu, F. Liu, M. Sasase, K. Ienaga, Y. Obata, R. Yukawa, K. Horiba, H. Kumigashira, S. Okuma, T. Inoshita, and H. Hosono, Sci. Adv. **5**, eaax9989 (2019).

[13] I. Klimovskikh, M. Otrokov, D. Estyunin, S. Eremeev, S. Filnov, A. Koroleva, E. Shevchenko, V. Voroshnin, I. Rusinov, M. Blanco-Rey, M. Hoffmann, Z. Aliev, M. Babanly, I. Amiraslanov, N. Abdullayev, V. Zverev, A. Kimura, O. Tereshchenko, K. A. Kokh, L. Petaccia, G. Di Santo, A. Ernst, P. Echenique, N. Mamedov, A. Shikin, and E. V. Chulkov, arXiv:1910.11653v1 (2019).

[14] S.-Y. Xu, M. Neupane, C. Liu, D. Zhang, A. Richardella, L. Andrew Wray, N. Alidoust, M. Leandersson, T. Balasubramanian, J. Sánchez-Barriga, O. Rader, G. Landolt, B. Slomski, J. Hugo Dil, J. Osterwalder, T.-R. Chang, H.-T. Jeng, H. Lin, A. Bansil, N. Samarth, and M. Zahid Hasan, Nat. Phys. **8**, 616 (2012).

[15] J. Zhang, C.-Z. Chang, P. Tang, Z. Zhang, X. Feng, K. Li, L.-l. Wang, X. Chen, C. Liu, W. Duan, K. He, Q.-K. Xue, X. Ma, and Y. Wang, Science **339**, 1582 (2013).

[16] A. J. Bestwick, E. J. Fox, X. Kou, L. Pan, K. L. Wang, and D. Goldhaber-Gordon, Phys. Rev. Lett. **114**, 187201 (2015).

[17] C.-Z. Chang, W. Zhao, D. Y. Kim, H. Zhang, B. A. Assaf, D. Heiman, S.-C. Zhang, C. Liu, M. H. W. Chan, and J. S. Moodera, Nat. Mater. **14**, 473 (2015).

[18] J. A. Krieger, C.-Z. Chang, M.-A. Husanu, D. Sostina, A. Ernst, M. M. Otrokov, T. Prokscha, T. Schmitt, A. Suter, M. G. Vergniory, E. V. Chulkov, J. S. Moodera, V. N. Strocov, and Z. Salman, Phys. Rev. B **96**, 184402 (2017).

[19] A. M. Shikin, A. A. Rybkina, D. A. Estyunin, D. M. Sostina, I. I. Klimovskikh, V. Y. Voroshnin, A. G. Rybkin, K. A. Kokh, O. E. Tereshchenko, L. Petaccia, G. Di Santo, A. Kimura, P. N. Skirdkov, K. A. Zvezdin, and A. K. Zvezdin, Sci. Rep. **8**, 6544 (2018).

[20] A. M. Shikin, A. A. Rybkina, D. A. Estyunin, D. M. Sostina, V. Y. Voroshnin, I. I. Klimovskikh, A. G. Rybkin, Y. A. Surnin, K. A. Kokh, O. E. Tereshchenko, L. Petaccia, G. Di Santo, P. N. Skirdkov, K. A. Zvezdin, A. K. Zvezdin, A. Kimura, E. V. Chulkov, and E. E. Krasovskii, Phys. Rev. B **97**, 245407 (2018).

[21] A. M. Shikin, D. A. Estyunin, Y. I. Surnin, A. V. Koroleva, E. V. Shevchenko, K. A. Kokh, O. E. Tereshchenko, S. Kumar, E. F. Schwier, K. Shimada, T. Yoshikawa, Y. Saitoh, Y. Takeda, and A. Kimura, Sci. Rep. **9**, 4813 (2019).

[22] S. O. Filnov, Y. A. Surnin, A. V. Koroleva, I. I. Klimovskikh, D. A. Estyunin, A. Y. Varykhalov, K. A. Bokai, K. A. Kokh, O. E. Tereshchenko, V. A. Golyashov, E. V. Shevchenko, and A. M. Shikin, J. Exp. Theor. Phys. **129**, 404 (2019).

[23] M. Mogi, R. Yoshimi, A. Tsukazaki, K. Yasuda, Y. Kozuka, K. S. Takahashi, M. Kawasaki, and Y. Tokura, Appl. Phys. Lett. **107**, 182401 (2015).

[24] I. Lee, C. K. Kim, J. Lee, S. J. L. Billinge, R. Zhong, J. A. Schneeloch, T. Liu, T. Valla, J. M. Tranquada, G. Gu, and J. C. S. Davis, Proc. Natl. Acad. Sci. U. S. A. **112**, 1316 (2015).

[25] Y. Tokura, K. Yasuda, and A. Tsukazaki, Nat. Rev. Phys. **1**, 126 (2019).

[26] S. V. Eremeev, M. M. Otrokov, and E. V. Chulkov, J. Alloys Compd. **709**, 172 (2017).

[27] D. Zhang, M. Shi, T. Zhu, D. Xing, H. Zhang, and J. Wang, Phys. Rev. Lett. **122**, 206401 (2019).

[28] J. Li, Y. Li, S. Du, Z. Wang, B.-L. Gu, S.-C. Zhang, K. He, W. Duan, and Y. Xu, Sci. Adv. **5**, eaaw5685 (2019).

[29] M. M. Otrokov, I. P. Rusinov, M. Blanco-Rey, M. Hoffmann, A. Y. Vyazovskaya, S. V. Eremeev, A. Ernst, P. M. Echenique, A. Arnau, and E. V. Chulkov, Phys. Rev. Lett. **122**, 107202 (2019).

[30] Z. S. Aliev, I. R. Amiraslanov, D. I. Nasonova, A. V. Shevelkov, N. A. Abdullayev, Z. A. Jahangirli, E. N. Orujlu, M. M. Otrokov, N. T. Mamedov, M. B. Babanly, and E. V. Chulkov, J. Alloys Compd. **789**, 443 (2019).

[31] B. Chen, F. Fei, D. Zhang, B. Zhang, W. Liu, S. Zhang, P. Wang, B. Wei, Y. Zhang, Z. Zuo, J. Guo, Q. Liu, Z. Wang, X. Wu, J. Zong, X. Xie, W. Chen, Z. Sun, S. Wang, Y. Zhang, M. Zhang, X. Wang, F. Song, H. Zhang, D. Shen, and B. Wang, Nat. Commun. **10**, 4469 (2019).

[32] Y. Deng, Y. Yu, M. Z. Shi, Z. Guo, Z. Xu, J. Wang, X. H. Chen, and Y. Zhang, Science **2020**, eaax8156.

[33] C. Liu, Y. Wang, H. Li, Y. Wu, Y. Li, J. Li, K. He, Y. Xu, J. Zhang, and Y. Wang, "Robust axion insulator and Chern insulator phases in a two-dimensional antiferromagnetic topological insulator," Nature Mater. (published online, 2020).

[34] J.-Q. Yan, Q. Zhang, T. Heitmann, Z. Huang, K. Y. Chen, J.-G. Cheng, W. Wu, D. Vaknin, B. C. Sales, and R. J. McQueeney, Phys. Rev. Mater. **3**, 064202 (2019).

[35] A. Zeugner, F. Nietschke, A. U. B. Wolter, S. Gass, R. C. Vidal, T. R. F. Peixoto, D. Pohl, C. Damm, A. Lubk, R. Hentrich, S. K. Moser, C. Fornari, C. H. Min, S. Schatz, K. Kissner, M. Ünzelmann, M. Kaiser, F. Scaravaggi, B. Rellinghaus, K. Nielsch, C. Hess, B. Büchner, F. Reinert, H. Bentmann, O. Oeckler, T. Doert, M. Ruck, and A. Isaeva, Chem. Mater. **31**, 2795 (2019).

[36] S. H. Lee, Y. Zhu, Y. Wang, L. Miao, T. Pillsbury, H. Yi, S. Kempinger, J. Hu, C. A. Heikes, P. Quarterman, W. Ratcliff, J. A. Borchers, H. Zhang, X. Ke, D. Graf, N. Alem, C.-Z. Chang, N. Samarth, and Z. Mao, Phys. Rev. Res. **1**, 012011 (2019).

[37] R. C. Vidal, H. Bentmann, T. R. F. Peixoto, A. Zeugner, S. Moser, C.-H. Min, S. Schatz, K. Kißner, M. Ünzelmann, C. I. Fornari, H. B. Vasili, M. Valvidares, K. Sakamoto, D. Mondal, J. Fujii, I. Vobornik, S. Jung, C. Cacho, T. K. Kim, R. J. Koch, C. Jozwiak, A. Bostwick, J. D. Denlinger, E. Rotenberg, J. Buck, M. Hoesch, F. Diekmann, S. Rohlf, M. Kalläne, K. Rossnagel, M. M. Otrokov, E. V. Chulkov, M. Ruck, A. Isaeva, and F. Reinert, Phys. Rev. B **100**, 121104 (2019).

[38] Y. Gong, J. Guo, J. Li, K. Zhu, M. Liao, X. Liu, Q. Zhang, L. Gu, L. Tang, X. Feng, D. Zhang, W. Li, C. Song, L. Wang, P. Yu, X. Chen, Y. Wang, H. Yao, W. Duan, Y. Xu, S.-C. Zhang, X. Ma, Q.-K. Xue, and K. He, Chin. Phys. Lett. **36**, 076801 (2019).

[39] Y.-J. Hao, P. Liu, Y. Feng, X.-M. Ma, E. F. Schwier, M. Arita, S. Kumar, C. Hu, R. Lu, M. Zeng, Y. Wang, Z. Hao, H.-Y. Sun, K. Zhang, J. Mei, N. Ni, L. Wu, K. Shimada, C. Chen, Q. Liu, and C. Liu, Phys. Rev. X **9**, 041038 (2019).

[40] Y. J. Chen, L. X. Xu, J. H. Li, Y. W. Li, H. Y. Wang, C. F. Zhang, H. Li, Y. Wu, A. J. Liang, C. Chen, S. W. Jung, C. Cacho, Y. H. Mao, S. Liu, M. X. Wang, Y. F. Guo, Y. Xu, Z. K. Liu, L. X. Yang, and Y. L. Chen, Phys. Rev. X **9**, 041040 (2019).

[41] H. Iwasawa, E. F. Schwier, M. Arita, A. Ino, H. Namatame, M. Taniguchi, Y. Aiura, and K. Shimada, Ultramicroscopy **182**, 85 (2017).

[42]M. Ye, T. Xu, G. Li, S. Qiao, Y. Takeda, Y. Saitoh, S.-Y. Zhu, M. Nurmamat, K. Sumida, Y. Ishida, S. Shin, and A. Kimura, Phys. Rev. B **99**, 144413 (2019).
[43]A. Chikina, M. Hoppner, S. Seiro, K. Kummer, S. Danzenbacher, S. Patil, A. Generalov, M. Guttler, Y. Kucherenko, E. V. Chulkov, Y. M. Koroteev, K. Koepernik, C. Geibel, M. Shi, M. Radovic, C. Laubschat, and D. V. Vyalikh, Nat. Commun. **5**, 3171 (2014).
[44]I. I. Klimovskikh, A. M. Shikin, M. M. Otrokov, A. Ernst, I. P. Rusinov, O. E. Tereshchenko, V. A. Golyashov, J. Sánchez-Barriga, A. Y. Varykhalov, O. Rader, K. A. Kokh, and E. V. Chulkov, Sci. Rep. **7**, 3353 (2017).
[45]P. Swatek, Y. Wu, L.-L. Wang, K. Lee, B. Schrunk, J. Yan, and A. Kaminski, arXiv:1907.09596v1 (2019).